A New Construction of Smooth Surfaces from Triangle Meshes Using Parametric Pseudo-Manifolds

Marcelo Siqueira[a,*], Dianna Xu[b], Jean Gallier[c], Luis Gustavo Nonato[d], Dimas Martínez Morera[e], Luiz Velho[f]

[a] *UFMS, Campo Grande (MS), Brazil, email:* marcelo@dct.ufms.br
[b] *Bryn Mawr College, Bryn Mawr (PA), USA, email:* dxu@cs.brynmawr.edu
[c] *University of Pennsylvania, Philadelphia (PA), USA, email:* jean@cis.upenn.edu
[d] *ICMC-USP, São Carlos (SP), Brazil, email:* gnonato@icmc.usp.br, *and Scientific Computing and Imaging Institute, University of Utah, Salt Lake City (UT), USA*
[e] *UFAL, Maceió (AL), Brazil, email:* dimasmm@impa.br
[f] *IMPA, Rio de Janeiro (RJ), Brazil, email:* lvelho@impa.br

Abstract

We introduce a new manifold-based construction for fitting a smooth surface to a triangle mesh of arbitrary topology. Our construction combines in novel ways most of the best features of previous constructions and, thus, it fills the gap left by them. We also introduce a theoretical framework that provides a sound justification for the correctness of our construction. Finally, we demonstrate the effectiveness of our manifold-based construction with a few concrete examples.

Key words:
Geometric Modeling, Manifolds, Triangle Meshes

1. Introduction

The problem of fitting a surface with guaranteed topology and continuity to the vertices of a polygonal mesh of arbitrary topology has been a topic of major research interest for many years. The main difficulty of this problem lies in the fact that, in general, meshes of arbitrary topology cannot be parametrized on a single rectangular domain and have no restriction on vertex connectivity. Most existing solutions rely on mathematical and computational frameworks capable of guaranteeing low degrees (i.e., C^2 and below) of continuity only. However, higher order surfaces are often required for certain numerical simulations and to meet visual, aesthetic, and functional requirements. While a few high order constructions do exist, most are expensive, complex, and/or difficult to implement.

Much of the previous research efforts has been focused on stitching parametric polynomial patches together along their seams, where each patch is the image of a distinct parametrization of a closed, planar domain. Because the patches need to be "pieced" together, ensuring continuity along the borders has proved to be a difficult problem, particularly for closed meshes. Although there is a large number of C^k/G^k constructions based on the "stitching" paradigm and catered to triangle meshes [1], only very few go beyond C^2-continuity [2, 3]. Existing constructions (even those C^2 and below) are typically complex, they lack shape control and cannot achieve good visual quality without additional processing. Very few were ever implemented and the degree of the polynomial patches required by most constructions grows rapidly with the desired order of continuity, which tend to yield surfaces with poor visual quality.

Subdivision surface is another popular approach which has been extensively investigated in the past 30 years [4, 5, 6, 7, 8, 9, 10]. These techniques are intuitive, simple to implement and in general produce smooth surfaces of good visual quality. However, constructions that go beyond C^2/G^2 are rare, and guaranteeing continuity around *extraordinary* vertices is difficult [11, 12]. Furthermore, previous efforts by Prautzsch and Reif [13, 14] indicate that subdivision schemes to produce C^k surfaces, for large k, cannot be as simple and elegant as existing C^1/G^1 and C^2/G^2 sub-

*Partially supported by CNPq (Grant 475703/2006-5). Address: *DCT-CCET-UFMS, Av. Costa e Silva, S/N, Cidade Universitária, Campo Grande, MS, Brazil, CEP: 79070-900, TEL/FAX: +55 67 3345 7515.*

division schemes.

Unlike the two aforementioned approaches, the manifold-based approach pioneered by Grimm and Hughes [15] has proved well-suited to fit, with relative ease, C^k-continuous parametric surfaces to triangle and quadrilateral meshes, including $k = \infty$ [15, 16, 17, 18]. The mathematical theory of manifolds was conceived with built-in arbitrary smoothness, and the differential structure of a manifold provides us with a natural setting for solving equations on surfaces. Manifold-based constructions also share some of the most important properties of splines surfaces, such as local shape control and fixed-sized local support for basis functions. Thus, as pointed out by Grimm and Zorin [19], a manifold is an attractive surface representation form for a handful of applications in graphics, such as reaction-diffusion texture, texture synthesis, fluid simulation, and surface deformation.

Unfortunately, existing manifold-based constructions present some drawbacks that limit their wide use in practical applications. In particular, constructions able to handle triangular meshes either make use of an intricate mechanism to define the manifold structure [15] or cannot guarantee smoothness in every point of the surface [18]. On the other hand, methods with a simpler construction [16] as well as arbitrary smoothness [17] do not establish a complete framework for handling triangular meshes.

1.1. Contributions

In this paper, we present a new manifold-based construction for fitting surfaces of arbitrary smoothness (i.e., C^∞-continuous) to triangle meshes. Our construction combines, in the same framework, most of the best features of previous constructions. In particular, it is more compact and simpler than the one in [15], more powerful than the construction in [18], and shares with [17], a construction devised for quadrilateral meshes, the ability of producing C^∞-continuous surfaces and the flexibility in ways of defining the geometry of the resulting surface. We also introduce a theoretical framework that provides a sound justification for the correctness of our manifold-based construction. This framework is a slight improvement upon the one given by Grimm and Hughes [15], which was used to undergird the constructions described in [15, 16, 17].

2. Prior Work

Extensive literature exists on fitting smooth surfaces from meshes. However, in order to better contextualize our approach, we focus this section on manifold-based techniques. For a more detailed review of the manifold-based approach and its applications, we refer the reader to [19].

The first manifold-based construction for surface modeling was proposed by Grimm and Hughes [15]. Their seminal work has since then been the basis of most subsequent constructions, including ours. Their construction takes a triangle mesh as input, subdivides by one step of Catmull-Clark subdivision scheme, and then considers the dual of the subdivided mesh (which is no longer a triangle mesh). Surface topology is defined from a structure they named *proto-manifold*, which contains a finite set A of connected open sets in $\mathbb{R}^2$ (the theory holds in $\mathbb{R}^n$ indeed) and a set of transition functions that, together with the mesh connectivity, dictate how the sets in A overlap with each other. Each type of mesh element (vertex, edge, and face) gives rise to a different open set, requiring the construction of three different types of transition functions. Geometry is added by handling the mesh geometry through control points and blending functions explicitly defined from the open sets. The construction in [15] yields C^2-continuous surfaces only, but it was later simplified and improved [20] to produce C^k-continuous surfaces, for any finite integer k. Subsequent efforts [16, 17] aimed at providing a construction that requires a smaller set of open sets, consists of simpler transition functions, and achieves C^∞-continuity.

Based on the concept of proto-manifold, Navau and Garcia [16] introduced a construction that takes a quadrilateral mesh and two integers, k and n, as input. The integer k specifies the desired degree of (finite) continuity, while n is related to the extent of the open sets in A. Their construction assigns an open set to each mesh vertex. Differently from [15], only two types of open sets are built, one associated with regular vertices (valence equal 4) and other with irregular vertices. However, three distinct types of transition functions are still needed so as to glue regular-regular, regular-irregular, and irregular-irregular open sets. The size of the set A grows with n, but it also depends on the mesh topology. In fact, it can be larger than the size of A in [15] even for smaller values of n. Geometry is defined quite similarly as in [15]. An extension of [16] to meshes of arbitrary topology has been proposed [21], but it shares with the construction in [16] the same advantages and drawbacks.

Ying and Zorin [17] devised a very elegant proto-manifold structure from quadrilateral meshes. Making use of only one type of open set and a simple analytical transition function, the resulting surface is C^∞-

continuous. This work improves upon the two previous techniques considerably. Another contribution is that control points are replaced by general polynomials, thus offering a more flexible control of the geometry of the resulting surface. Their construction can be extended to deal with triangle meshes, but one has to work out certain elements of its proto-manifold, which are not entirely obvious.

More recently, Gu, He, and Qin [18] introduced a triangle-based manifold construction called *manifold splines*, which is based on a theoretical framework of its own. This construction employs affine transform as transition functions and (rational) polynomial functions to derive the geometry. This is the first manifold-based construction to yield a purely (rational) polynomial surface. Having a surface specified by a (rational) polynomial expression is very desirable in practice. However, as closed surfaces (except tori) cannot be covered by an "affine atlas" (see [22]), singular points not belonging to any open set must appear on the surface, thereby affecting the visual quality in the vicinity of these points. Making use of discrete Ricci flow, Gu et al. [23] have improved the manifold spline construction to reduce to only one singular point on the entire surface.

Our construction is based on the theoretical framework developed by Grimm and Hughes [15], yet it differs from the aforementioned constructions in the following aspects: the proto-manifold counterpart of our construction is given two additional conditions that render it more general and stronger than the proto-manifold in [15]. As in [17], our construction also has only one type of open set and (simple) transition function, can produce C^∞ surfaces, and defines the geometry of the resulting surfaces using polynomials. Differently from Ying and Zorin [17], our construction is devised to work with triangle meshes, which are far more popular than quadrilateral meshes in graphics applications [24]. In addition, we define geometry from simpler polynomials (i.e., rectangular Bézier patches) which means that the resulting surface is contained in the convex hull of all control points defining its patches. This property allows us to optimize for speed ray tracing and collision detection algorithms. The surfaces produced by our construction are not polynomial, but they do not contain any singular points. Finally, our construction is simple to implement.

3. Mathematical Background

The formal definition of a manifold can be found in standard mathematics textbooks, such as [25]. Informally, manifolds are spaces that locally behave like the familiar n-dimensional Euclidean space, and on which we can do calculus (e.g., compute derivatives, integrals, volumes, and curvatures). For that, each manifold, M, is equipped with an *atlas*, which is a collection of *charts*. Each chart is a pair (U, φ), where U is an open set of M and $\varphi : U \to \varphi(U) \subseteq \mathbb{R}^n$ is a homeomorphism. Furthermore, the charts of an atlas must cover M. The open sets, U_1 and U_2, of any two distinct charts, (U_1, φ_1) and (U_2, φ_2), may overlap (see Figure 1). *Transition functions*, $\varphi_{21} : \varphi_1(U_1 \cap U_2) \to \varphi_2(U_1 \cap U_2)$ and $\varphi_{12} : \varphi_2(U_1 \cap U_2) \to \varphi_1(U_1 \cap U_2)$, are defined to move between the overlapped regions consistently. These functions are required to satisfy two conditions: $\varphi_{21} = \varphi_2 \circ \varphi_1^{-1}$ and $\varphi_{12} = \varphi_1 \circ \varphi_2^{-1}$. Basically, functions φ_{21} and φ_{12} define which points in $\varphi_1(U_1 \cap U_2)$ and $\varphi_2(U_1 \cap U_2)$ correspond to the same point in M under φ_1^{-1} and φ_2^{-1}. Transition functions are often required to be C^k-continuous, so that the necessary degree of "smoothness" to compute differential properties of M is ensured.

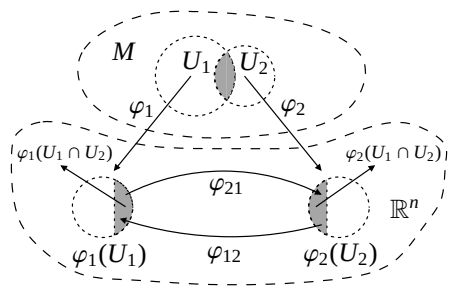

Figure 1: Constituents of a manifold.

A manifold-based approach for surface construction requires first building a manifold, M, which is a smooth surface in $\mathbb{R}^3$. The classic definition of a manifold assumes the existence of a manifold *a priori*, which is not very helpful from the constructive point of view. Fortunately, it is possible to define M in a constructive manner from a set of *gluing data* and a set of *parametrizations* (see Figure 2).

Definition 1. *Let n be an integer with $n \geq 1$ and let k be either an integer with $k \geq 1$ or $k = \infty$. A* set of gluing data *is a triple,*

$$\mathcal{G} = \left((\Omega_i)_{i \in I}, (\Omega_{ij})_{(ij) \in I \times I}, (\varphi_{ji})_{(i,j) \in K}\right),$$

satisfying the following properties, where I and K are (possibly infinite) countable index sets, and I is non-empty:

1. *For every $i \in I$, the set Ω_i is a non-empty open subset of $\mathbb{R}^n$ called* parametrization domain, *for short,*

p-domain, and the Ω_i are pairwise disjoint (i.e., $\Omega_i \cap \Omega_j = \emptyset$ for all $i \neq j$).

2. *For every pair $(i, j) \in I \times I$, the set Ω_{ij} is an open subset of Ω_i. Furthermore, $\Omega_{ii} = \Omega_i$ and $\Omega_{ji} \neq \emptyset$ if and only if $\Omega_{ij} \neq \emptyset$. Each non-empty Ω_{ij} (with $i \neq j$) is called a* gluing domain.
3. *If we let*

$$K = \{(i, j) \in I \times I \mid \Omega_{ij} \neq \emptyset\},$$

then $\varphi_{ji} : \Omega_{ij} \to \Omega_{ji}$ is a C^k bijection for every $(i, j) \in K$ called a transition function *(or* gluing function*) and the following conditions hold:*
   (a) $\varphi_{ii} = \mathrm{id}_{\Omega_i}$, *for all $i \in I$,*
   (b) $\varphi_{ij} = \varphi_{ji}^{-1}$, *for all $(i, j) \in K$, and*
   (c) *For all i, j, k, if $\Omega_{ji} \cap \Omega_{jk} \neq \emptyset$, then $\varphi_{ji}^{-1}(\Omega_{ji} \cap \Omega_{jk}) \subseteq \Omega_{ik}$ and $\varphi_{ki}(x) = \varphi_{kj} \circ \varphi_{ji}(x)$, for all $x \in \varphi_{ji}^{-1}(\Omega_{ji} \cap \Omega_{jk})$.*
4. *For every pair $(i, j) \in K$, with $i \neq j$, for every $x \in \partial(\Omega_{ij}) \cap \Omega_i$ and $y \in \partial(\Omega_{ji}) \cap \Omega_j$, there are open balls, V_x and V_y, centered at x and y, so that no point of $V_y \cap \Omega_{ji}$ is the image of any point of $V_x \cap \Omega_{ij}$ by φ_{ji}.*

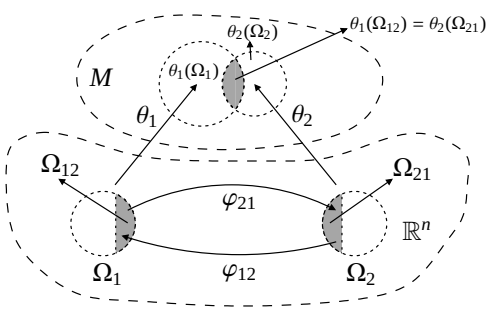

Figure 2: Constituents of a parametric pseudo-manifold.

There is a simple correspondence between the constituents of the traditional definition of a manifold and the ones of a set of gluing data and a set of parametrizations:

- each p-domain, $\Omega_i \subseteq \mathbb{R}^n$, is the image, $\Omega_i = \varphi_i(U_i)$, of an open set, U_i, of M under the map φ_i of the chart (U_i, φ_i) of an atlas of M;
- each gluing domain, $\Omega_{ij} \subseteq \Omega_i$, is the image, $\Omega_{ij} = \varphi_i(U_i \cap U_j)$, of the overlapping subset, $U_i \cap U_j$, of U_i and U_j under the map φ_i of the chart (U_i, φ_i) of an atlas of M;
- each transition function, $\varphi_{ij} : \Omega_{ji} \to \Omega_{ij}$, is a function from $\varphi_j(U_i \cap U_j) = \Omega_{ji}$ to $\varphi_i(U_i \cap U_j) = \Omega_{ij}$; and
- each parametrization, $\theta_i : \Omega_i \to M$, is the inverse, φ_i^{-1}, of the map $\varphi_i : U_i \to \mathbb{R}^n$, of the chart, (U_i, φ_i).

Condition 3(c) is called the *cocycle condition* and it plays a crucial role in Theorem 1, which states that an n-dimensional C^k manifold can be constructed from a set of gluing data. In turn, condition 4 ensures that the resulting manifold is Hausdorff. There are two subtle differences between our definition of gluing data and the definition of a proto-manifold in [15]. First, our cocycle condition (see Definition 1) is stronger than the one in [15], as the latter does not always guarantee that a (valid) manifold can be constructed from a proto-manifold (see [26]). Second, in the definition of a proto-manifold, there is no condition similar to condition 4. In order to ensure that the manifold built from a proto-manifold is Hausdorff, Grimm and Hughes [15] require that the manifold be embeddable in $\mathbb{R}^n$. This requirement is stronger than condition 4, as it prevents us from obtaining certain manifolds such as a 2-sphere resulting from gluing two open discs in $\mathbb{R}^2$ along an annulus.

Theorem 1. *For every set of gluing data,*

$$\mathcal{G} = ((\Omega_i)_{i \in I}, (\Omega_{ij})_{(i,j) \in I \times I}, (\varphi_{ji})_{(i,j) \in K}),$$

there is an n-dimensional C^k manifold, $M_{\mathcal{G}}$, whose transition functions are the φ_{ji}'s.

Proof. See [26] for a proof. □

Our proof of Theorem 1 in [26] gives us a theoretical construction, which yields an "abstract" manifold, $M_{\mathcal{G}}$, but no information on the geometry of this manifold. Furthermore, $M_{\mathcal{G}}$ may not be orientable or compact. However, for the problem we are dealing with, we are given a triangle mesh and we want to build a "concrete" manifold: a surface in $\mathbb{R}^3$ that approximates the given mesh. It turns out that it is always possible to define a *parametric pseudo-manifold* from any given set of gluing data, whose *image* in $\mathbb{R}^3$ is a surface if certain conditions hold.

Definition 2. *Let n and d be two integers with $n > d \geq 1$ and let k be integer with $k \geq 1$ or $k = \infty$. A* parametric C^k pseudo-manifold of dimension d in $\mathbb{R}^n$, *$\mathcal{M}$, is a pair,*

$$\mathcal{M} = (\mathcal{G}, (\theta_i)_{i \in I}),$$

where $\mathcal{G} = ((\Omega_i)_{i \in I}, (\Omega_{ij})_{(i,j) \in I \times I}, (\varphi_{ji})_{(i,j) \in K})$ is a set of gluing data, for some finite set I, and each θ_i is a C^k function, $\theta_i : \Omega_i \to \mathbb{R}^n$, called a parametrization *such that*

$$\theta_i = \theta_j \circ \varphi_{ji},$$

for all $(i, j) \in K$*. The subset,* $M \subset \mathbb{R}^n$*, given by*

$$M = \bigcup_{i \in I} \theta_i(\Omega_i)$$

is called the image *of the parametric pseudo-manifold,* $\mathcal{M}$*.*

When $d = 2$ and $n = 3$ in Definition 2, we call $\mathcal{M}$ a *parametric pseudo-surface*. If we require the θ_i's to be bijective and to further satisfy two conditions, (1) $\theta_i(\Omega_i) \cap \theta_j(\Omega_j) = \theta_i(\Omega_{ij}) = \theta_j(\Omega_{ji})$, for all $(i, j) \in K$, and (2) $\theta_i(\Omega_i) \cap \theta_j(\Omega_j) = \emptyset$, for all $(i, j) \notin K$, then the image, M, of the parametric pseudo-surface, $\mathcal{M}$, is guaranteed to be a surface in $\mathbb{R}^3$ [26].

4. Overview of the Construction Process

Recall that our goal is to fit a surface, $S \in \mathbb{R}^3$, to a triangle mesh $\mathcal{T}$. More specifically, we want to build a surface S that approximates the vertices of $\mathcal{T}$ and has the same topology as the underlying space, $|\mathcal{T}|$, of $\mathcal{T}$ (i.e., $|\mathcal{T}|$ is the point set resulting from the union of all points in the vertices, edges, and triangles of $\mathcal{T}$). We also assume that $|\mathcal{T}|$ is a surface in $\mathbb{R}^3$ with empty boundary. To build S, our construction defines a set of gluing data and a set of parametrizations. The set of gluing data,

$$\mathcal{G} = ((\Omega_i)_{i \in I}, (\Omega_{ij})_{(i,j) \in I \times I}, (\varphi_{ji})_{(i,j) \in K}),$$

is defined from the elements of $\mathcal{T}$. More specifically, let I be the set of vertices of $\mathcal{T}$. Then, we define a p-domain, Ω_u, for each $u \in I$. For any $u, v \in I$, we also define the gluing domains, Ω_{uv} and Ω_{vu}, such that $\Omega_{uv} = \emptyset$ if and only if $\Omega_{uv} = \emptyset$. Finally, for $u, v \in I$ such that $\Omega_{uv} \neq \emptyset$ (or equivalently, $\Omega_{vu} \neq \emptyset$), we define the transition functions

$$\varphi_{vu} : \Omega_{uv} \to \Omega_{vu} \quad \text{and} \quad \varphi_{uv} : \Omega_{vu} \to \Omega_{uv}.$$

In turn, the set of parametrizations is defined by creating local approximations to another surface defined on $\mathcal{T}$. More specifically, we first obtain a curved surface approximation to $|\mathcal{T}|$. This step is very flexible and can be done a number of ways (see Section 6). Next, for each p-domain Ω_u, we define a *shape function*, $\psi_u : \mathbb{R}^2 \to \mathbb{R}^3$, as a rectangular Bézier patch that locally approximates the surface defined on $\mathcal{T}$. We also define a non-negative *weight function*, $\gamma_u : \mathbb{R}^2 \to \mathbb{R}$, with compact support equal to the closure of Ω_u (i.e., γ_u is zero outside or on the boundary of Ω_u and greater than zero inside). Finally, the parametrization, θ_u, of each Ω_u is defined as a convex sum over all overlapping p-domains. In particular, for each point $x \in \Omega_u$, we have

$$\theta_u(x) = \sum_{v \in J_u(x)} \omega_{uv}(x) \cdot \psi_v \circ \varphi_{vu}(x), \tag{1}$$

where

$$\omega_{uv}(x) = \frac{\gamma_v \circ \varphi_{vu}(x)}{\sum_{w \in J_u(x)} \gamma_w \circ \varphi_{wu}(x)} \tag{2}$$

and

$$J_u(x) = \{v \mid x \in \Omega_{uv}\} \subseteq I.$$

The set $J_u(x)$ contains the index of each p-domain, Ω_v, that is "glued" to Ω_u at x by φ_{vu}. Note that $\varphi_{vu}(x)$ is the point in Ω_v identified with x by φ_{vu}. The former point is assigned a weight, $\omega_{uv}(x)$, which can be viewed as its contribution to $\theta_u(x)$. So, $\theta_u(x)$ adds up the contribution of each shape function, γ_v, defined in a p-domain that contains a point, $\varphi_{vu}(x)$, identified with x in the gluing process.

We can show that

$$\sum_{v \in J_u(x)} \omega_{uv}(x) = 1, \text{ with } \omega_{uv}(x) \geq 0,$$

and

$$\theta_u(x) = \theta_v \circ \varphi_{vu}(x),$$

which ensure that the expression defining θ_u is a convex sum and that $\theta_u(x)$ and $\theta_v \circ \varphi_{vu}(x)$ are the same point in $\mathbb{R}^3$. Finally, our smooth "surface" S is defined as the image,

$$S = \bigcup_{v \in I} \theta_v(\Omega_v), \tag{3}$$

of the parametric pseudo-surface, $\mathcal{M} = (\mathcal{G}, \theta_u)_{u \in I}$. Note that the continuity of S is determined by the lowest order of continuity of all its component functions. Since all of our transition functions, shape functions and weight functions are C^∞, so is our entire resulting surface.

5. Building a Set of Gluing Data

To build the set of gluing data, $\mathcal{G}$, we must define its collection of p-domains, gluing domains, and transition functions. These collections are defined in terms of two abstractions, a P-polygon and its canonical triangulation, and a bijective function. Now, we describe these elements. Recall that I is the index set consisting of the vertices of $\mathcal{T}$. Let $l : I \to \{1, \ldots, |I|\}$ be a map that assigns a unique *label* from $\{1, \ldots, |I|\}$ with each vertex, u, in I.

For each vertex u of $\mathcal{T}$, the *P-polygon, P_u, associated with u* is the regular polygon in $\mathbb{R}^2$ given by the vertices

$$u'_i = \left(2 \cdot l(u) + \cos\left(\frac{2\pi \cdot i}{m_u}\right), \sin\left(\frac{2\pi \cdot i}{m_u}\right)\right),$$

for each $i \in \{0, \ldots, m_u - 1\}$, where m_u is the valence of u (see Figure 3).

Definition 3. *For every $u \in I$, the p-*domain Ω_u *is the set*

$$\Omega_u = \left\{(x, y) \in \mathbb{R}^2 \mid (x - 2 \cdot l(u))^2 + y^2 < [\cos(\pi/m_u)]^2\right\},$$

where m_u is the valence of vertex u. Note that Ω_u is the interior, int(C_u), of the circle, C_u, inscribed in the P-polygon, P_u.

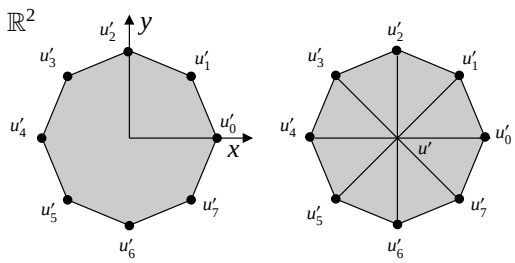

Figure 3: A P-polygon (left) and its canonical triangulation (right).

Note that every p-domain is a non-empty, open set of $\mathbb{R}^2$. Furthermore, for any two $v, w \in I$, with $v \neq w$, the p-domains Ω_v and Ω_w must be disjoint, as they reside inside P_v and P_w, respectively, whose interiors are disjoint. So, the collection, $\{\Omega_u\}_{u \in I}$, of p-domains satisfies condition 1 of Definition 1. To build gluing domains and transition functions, we define a triangulation of the P-polygons and a bijective function that is a composition of two rotations, an analytic function, and a double reflection.

We can triangulate P_u by adding m_u diagonals and the vertex, $u' = (2 \cdot l(u), 0)$, to P_u. Each diagonal connects u' to a vertex, u'_i, of P_u, for each $i = 0, \ldots, m_u - 1$. The resulting triangulation, denoted by T_u, is called the *canonical triangulation of P_u* (see Figure 3). Denote the set of vertices of T_u by $V(T_u)$, and let $\mathcal{N}(u, \mathcal{T})$ be the subset of vertices of $\mathcal{T}$ such that $v \in \mathcal{N}(u, \mathcal{T})$ if and only if $v = u$ or v is a vertex connected to u by an edge, $[u, v]$, of $\mathcal{T}$. Then, we can define a bijection, $s_u : \mathcal{N}(u, \mathcal{T}) \to V(T_u)$, such that $s_u(u) = u'$ and $[u, u_i, u_{i+1}]$ is a triangle in $\mathcal{T}$ if and only if $[s_u(u) = u', s_u(u_i), s_u(u_{i+1})]$ is a triangle in T_u, where $i = 0, 1, \ldots, m_u - 1$ and $i + 1$ should be considered congruent modulo m_u. We can extend the bijection s_u to map triangles incident to u in $\mathcal{T}$ onto triangles in T_u. In particular, if $\sigma = [u, u_i, u_{i+1}]$ is a triangle of $\mathcal{T}$ then $s_u(\sigma) = [u', s_u(u_i), s_u(u_{i+1})]$ is its corresponding triangle in T_u. Unless explicitly stated otherwise, we may occasionally denote vertex $s_u(v)$ by v', for every $v \in \mathcal{N}(u, \mathcal{T})$.

For each u in I and for each $p \in \mathbb{R}^2$, with $p \neq (2 \cdot l(u), 0)$, let $g_u : \mathbb{R}^2 - \{(2 \cdot l(u), 0)\} \to \mathbb{R}^2 - \{(0, 0)\}$ be given by

$$g_u(p) = f_u \circ t_u(p), \tag{4}$$

where $t_u : \mathbb{R}^2 \to \mathbb{R}^2$ is the unique rigid transformation (i.e., a translation) that takes $(2 \cdot l(u), 0)$ to the origin, $(0, 0)$, of $\mathbb{R}^2$, and $f_u : \mathbb{R}^2 - \{(0, 0)\} \to \mathbb{R}^2 - \{(0, 0)\}$ is given by

$$f_u(q) = g_u((\theta, r)) = \left(\frac{6}{m_u} \cdot \theta, \frac{\cos(\pi/6)}{\cos(\pi/m_u)} \cdot r\right), \tag{5}$$

where (θ, r) are the polar coordinates of $q \in \mathbb{R}^2 - \{(0, 0)\}$. Function g_u has the following interpretation (refer to Figure 4): it maps the interior of the circular sector, A, of C_u onto the interior of the circular sector, B, of the circle of radius $\cos(\pi/6)$ and centers at $(0, 0)$, where A is such that $t_u(A)$ (i.e., the translation of A given by t_u) consists of $(0, 0)$ and all points with polar coordinates $(\theta, r) \in [-2\pi/m_u, 2\pi/m_u] \times (0, \cos(\pi/m_u)]$ and B consists of $(0, 0)$ and all points with polar coordinates $(\beta, s) \in [-\pi/3, \pi/3] \times (0, \cos(\pi/6)]$. We say that B is the *canonical sector*. Note that g_u is a bijection. Its inverse, g_u^{-1}, is given by

$$g_u^{-1}(q) = t_u^{-1} \circ f_u^{-1}(q), \tag{6}$$

where

$$f_u^{-1}(q) = f_u^{-1}((\beta, s)) = \left(\frac{m_u}{6} \cdot \theta, \frac{\cos(\pi/m_u)}{\cos(\pi/6)} \cdot s\right), \tag{7}$$

for every $q \in \mathbb{R}^2 - \{(0, 0)\}$ with polar coordinates (β, s).

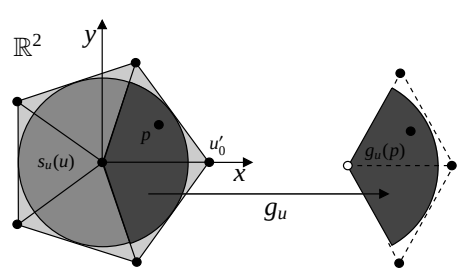

Figure 4: The action of g_u upon a point $p \in C_u$.

Let $h : \mathbb{R}^2 \to \mathbb{R}^2$ be the function

$$h(p) = h((x, y)) = (1 - x, -y), \tag{8}$$

for every point $p \in \mathbb{R}^2$ with rectangular coordinates (x, y). Function h is a "double" reflection: $p = (x, y)$ is reflected over the line $x = 0.5$ and then over the line $y = 0$.

Finally, for any two vertices u, v of $\mathcal{T}$ such that $[u, v]$ is an edge of $\mathcal{T}$, let

$$g_{(u,v)} : C_u - \{(2 \cdot l(u), 0)\} \to C_v - \{(2 \cdot l(v), 0)\}$$

be the composite function given by

$$g_{(u,v)}(p) = R^{-1}_{(v,u)} \circ g_v^{-1} \circ h \circ g_u \circ R_{(u,v)}(p)\,, \qquad (9)$$

for every $p \in C_u - \{(2 \cdot l(u), 0)\}$, where $R_{(u,v)}$ is a rotation around $(2 \cdot l(u), 0)$ that identifies the edge $[s_u(u) = u', s_u(v)]$ of T_u with its edge $[u', u'_0]$. Likewise, $R^{-1}_{(v,u)}$ is a rotation around $(2 \cdot l(v), 0)$ that identifies the edge $[s_v(v) = v', v'_0]$ of T_v with its edge $[v', v'_j]$, where $j \in \{0, 1, \ldots, m_v - 1\}$ and $s_v(v'_j) = u$. Figure 5 shows the action of $g_{(u,v)}$ upon a given point p in the set $C_u - \{(2 \cdot l(u), 0)\}$.

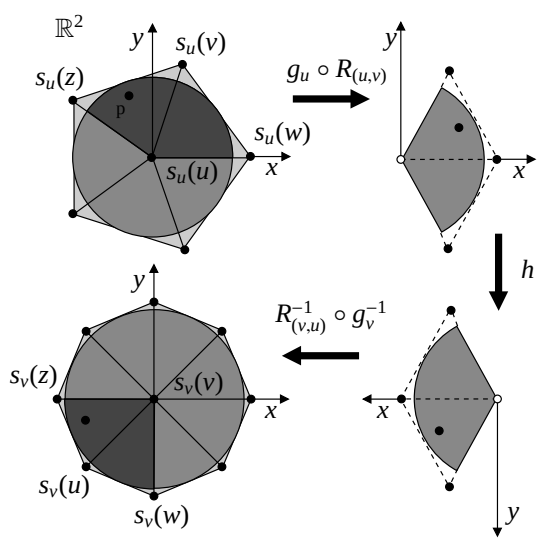

Figure 5: The action of $g_{(u,v)}$ upon a point $p \in C_u$.

Function $g_{(u,v)}$ also has the following interpretation: it maps the interior of a sector, A, of C_u onto the interior of a sector, B, of C_v. These two sectors are closely related. Let w and z be the two vertices of $\mathcal{T}$ such that $[u, v, w]$ and $[u, v, z]$ are the two triangles of $\mathcal{T}$ sharing the edge $[u, v]$. Then, sector A is the circular sector of C_u contained in the quadrilateral $[s_u(u) = u', s_u(w), s_u(v), s_u(z)]$, while sector B is the circular sector of C_v contained in the quadrilateral $[s_v(v) = v', s_v(z), s_v(u), s_v(w)]$. Function $g_{(u,v)}$ is also a bijection, and its inverse, $g^{-1}_{(u,v)}$, is equal to the function $g_{(v,u)}$:

$$g_{(v,u)}(q) = R^{-1}_{(u,v)} \circ g_u^{-1} \circ h \circ g_v \circ R_{(v,u)}(q)\,, \qquad (10)$$

for every $q \in C_v - \{(2 \cdot l(v), 0)\}$. Function $g_{(u,v)}$ plays a crucial role in the definitions of gluing domains and transition functions.

Definition 4. *For any $u, v \in I$, the* gluing domain Ω_{uv} *is defined as*

$$\Omega_{uv} = \begin{cases} g_{uv}^{-1}(g_{uv}(\Omega_u) \cap \Omega_v) & \text{if } [u, v] \text{ is an edge of } \mathcal{T}, \\ \emptyset & \text{otherwise.} \end{cases}$$

Although it is not obvious to see, the above definition of gluing domain satisfies condition 2 of Definition 1 [26]. In particular, the fact that $\Omega_{uv} = \emptyset$ if and only if $\Omega_{vu} = \emptyset$ is crucial to defining transition functions in a consistent manner. In what follows we give the formal definition of a transition function in our construction:

Definition 5. *Let K be the index set,*

$$K = \{(u, v) \in I \times I \mid \Omega_{uv} \neq 0\}\,.$$

Then, for any pair $(u, v) \in K$, the transition function,

$$\varphi_{vu} : \Omega_{uv} \to \Omega_{vu}\,,$$

is such that, for every $p \in \Omega_{uv}$, we let $\varphi_{vu}(p) = g_{uv}(p)$.

Figure 6 illustrates Definition 5.

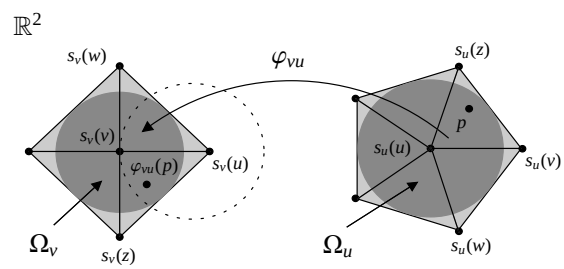

Figure 6: Illustration of Definition 5.

It is important to emphasize that our transition functions are bijective and C^∞-continuous, as function g_{uv} is defined as a composition of C^∞-continuous, bijective functions. In addition, they satisfy condition 3 of Definition 1 [26].

6. Building Parametrizations

Let $\mathcal{G}$ be a set of gluing data built from a triangle mesh, $\mathcal{T}$, as in Section 5. We want to define a family of parametrizations, $\{\theta_{(\sigma,u)}\}_{(\sigma,u)\in I}$, from $\mathcal{G}$. For now,

we assume that we are given a surface, $S' \subset \mathbb{R}^3$, that approximates $|\mathcal{T}|$. More specifically, we assume that S' is the union of finitely many parametric patches, $b_\sigma : \mathbb{R}^2 \to \mathbb{R}^3$, each of which is associated with a triangle, σ, of $\mathcal{T}$ and all of them are defined in an affine frame, $\triangle \subset \mathbb{R}^2$:

$$S' = \bigcup_{\sigma \in \mathcal{T}} b_\sigma(\triangle)\,.$$

In addition, we require S' be at least C^0-continuous. We can view S' as describing the geometry we want to locally approximate with the parametrizations in $\{\theta_{(\sigma,u)}\}_{(\sigma,u)\in I}$. To define each parametrization $\theta_{(\sigma,u)}$, we need to specify a family, $\{\psi_{(\sigma,u)}\}_{(\sigma,u)\in I}$, of shape functions and a family, $\{\gamma_{(\sigma,u)}\}_{(\sigma,u)\in I}$, of weight functions (see Eq. (1)).

Definition 6. *For each $u \in I$, we define the* shape function,

$$\psi_u : \mathbb{R}^2 \to \mathbb{R}^3\,,$$

associated with Ω_u *as the Bézier surface patch of bi-degree* (m, n),

$$\psi_u(p) = \sum_{0\le j\le m} \sum_{0\le k\le n} b^u_{j,k} \cdot B^m_j(x) \cdot B^n_k(y)\,,$$

where (x, y) are the coordinates of $p \in \mathbb{R}^2$ with respect to the affine frame $[-L + 2 \cdot l(u), -L] \times [L + 2 \cdot l(u), L]$, with $L = \cos(\pi/m_u)$, $\{b^u_{j,k}\} \subset \mathbb{R}^3$ are the control points, *and*

$$B^l_i(t) = \binom{l}{i}\left(\frac{r-t}{r-s}\right)^{l-i}\left(\frac{t-s}{r-s}\right)^{i}$$

is the i-th Bernstein polynomial of degree l over the affine frame $[s, r]$, *for every $i \in \{0, 1, \ldots, l\}$. We let the bi-degree, (m, n), of ψ_u be $(m_u + 1, m_u + 1)$, where m_u is the valence of u.*

The controls points are determined by solving a least squares fitting problem. In particular, $\{b^u_{j,k}\}$ is the family of control points that uniquely defines a Bézier patch of bi-degree (m, n) (i.e., $\psi_{(\sigma,u)}$) which best fits (*in a least squares sense*) a finite set, P, of pairs, (q, p), of points, where q belongs to P_u and p belongs to the surface S'. We compute P iteratively by starting with $P = \emptyset$ and then proceeding as follows:

- We uniformly sample the quadrilateral $\square_u = [-L + 2 \cdot l(u), -L] \times [L + 2 \cdot l(u), L] \subset \mathbb{R}^2$ to generate a set, $Q \subset P_u$, with $4 \cdot (m_u + 1)^2$ points. Note that $\square_u$ is the smallest quadrilateral that contains Ω_u. Note also that a uniform sampling of $\square_u$ will contain points that are not in P_u. These points are not placed into Q.
- For each point $q \in Q$, we find the triangle τ of $\mathcal{T}$ such that q is contained in the triangle $s_u(\tau)$ of T_u. Then, we compute the barycentric coordinates, (λ, ν, η), of q with respect to $s_u(\tau)$ and use these coordinates to compute a point, $r = \lambda \cdot a + \nu \cdot b + \eta \cdot c$, in $\triangle = [a, b, c]$, where $\triangle$ is the common affine frame of all parametric patches defining S'. To compute (λ, ν, η) in a consistent manner, we must fix an ordering for the vertices of $\triangle$ and for the vertices of each $s_u(\tau)$, so that we know which coordinate is associated with each vertex of $s_u(\tau)$ and $\triangle$. Finally, we compute $b_\tau(r)$, let $p = b_\tau(r)$, and add the pair, (q, p), to P. Figure 7 illustrates the computation of q and p.

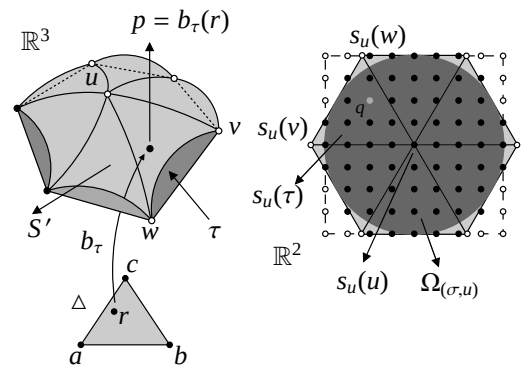

Figure 7: Local sampling of S' (white-filled vertices are not in Q).

Once P is computed, we use a standard least squares fitting procedure to compute $\{b^u_{j,k}\}$ (see [1], p. 278). To define the family, $\{\gamma_{(\sigma,u)}\}_{(\sigma,u)\in I}$, of weight functions, we first need specify two functions. For every $t \in \mathbb{R}$, let $h : \mathbb{R} \to \mathbb{R}$ and $\xi : \mathbb{R} \to \mathbb{R}$ be two functions defined as follows:

$$h(t) = \begin{cases} 1 & \text{if } t \le 0 \\ 0 & \text{if } t \ge 1 \\ e^{\dfrac{2 \cdot e^{-1/t}}{t-1}} & \text{otherwise} \end{cases} \tag{11}$$

and

$$\xi(t) = \begin{cases} 1 & \text{if } t \le L_1 \\ 0 & \text{if } t \ge L_2 \\ \dfrac{h(L)}{h(L) + h(1-L)} & \text{otherwise}\,, \end{cases} \tag{12}$$

where L_1, L_2 are constant, with $0 < L_1 < L_2 < 1$, and $L = (t - L_1)/(L_2 - L_1)$. Function ξ was borrowed from [17]. Note that $\xi(t)$ is constant for $t \le L_1$ and $t \ge L_2$, and it is strictly decreasing when t varies from L_1 to L_2. Function $\xi(t)$ is C^∞, and its i-th derivative,

$D^i\xi(t)$, vanishes for $t \leq L_1$ and $t \geq L_2$, and it is nonzero for $t \in (L_1, L_2) \subset \mathbb{R}$. Figure 8 shows a plot of $\xi(t)$, for $t \in [0, 1]$.

Definition 7. *For each $u \in I$, the* weight function,

$$\gamma_u : \mathbb{R}^2 \to \mathbb{R},$$

associated with Ω_u *is given by*

$$\gamma_u(p) = \xi(\|p - (2 \cdot l(u), 0)\|),$$

for every $p \in \mathbb{R}^2$, where $\|p - (2 \cdot l(u), 0)\|$ is the Euclidean distance from p to the center, $(2 \cdot l(u), 0)$, of the inscribed circle, C_u, of P_u, and the constants L_1 and L_2 (in the definition of ξ) are set to $0.25 \cdot L_2$ and $\cos(\pi/m_u)$, respectively.

By construction, function γ_u is positive for all points inside its *support*, *supp*(γ_u), which is the p-domain Ω_u. Note that γ_u attains its maximum, which is equal to 1, at $p = (2 \cdot l(u), 0)$ and in the neighborhood of p given by $\{q \in \Omega_u \mid \|p - q\| < L_1\}$. Moreover, function γ_u decreases as p moves towards the boundary of Ω_u and vanishes outside Ω_u. This is because $\|p - q\| \geq L_2$, for every point $q \in \mathbb{R}^2$ on the boundary of Ω_u or outside it. So, γ_u is non-negative and its support, *supp*(γ_u), is compact.

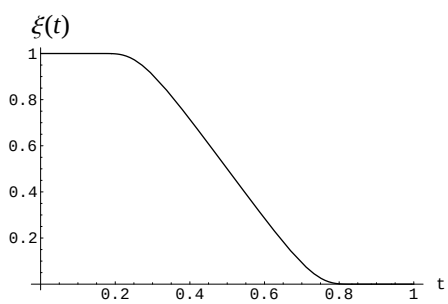

Figure 8: Plot of $\xi(t)$ for $t \in (0, 1) \subset \mathbb{R}$, using $L_1 = 0.2$ and $L_2 = 0.8$.

7. Implementation Details and Results

To implement our manifold-based construction, we augmented a simple object-oriented, topological data structure, such as a DCEL [27], to store the information about the set of gluing data, $\mathcal{G}$, and the family of parametrizations, $\{\theta_{(\sigma,u)}\}_{(\sigma,u)\in I}$. It is worth mentioning that there is no need to explicitly compute and store p-domains, gluing domains, P-polygons and their associated triangulations. Transition functions, shape functions, and weight functions become "methods" associated with the edges and vertices of the data structure. Our implementation also provides the "user" with a method to compute a point p in the parametric pseudo-surface, S, as given by Eq. (3). This method hides from the user the fact that S is the union of a collection of parametrizations. In other words, the user does not have to know about the existence of gluing data and parametrizations. In particular, the user provides the method with a triangle, σ, of $\mathcal{T}$ and a point, p, in σ such that $p = \lambda \cdot u + \nu \cdot v + \eta \cdot w$, where u, v, w are the vertices of σ and λ, ν, and η are the barycentric coordinates of p with respect to u, v, w, in this order. The idea behind our method is to map p to a point in either Ω_u, Ω_v, or Ω_w. To do so in a consistent manner, we fix a vertex, say u, of σ and always map p to the point $q = \lambda \cdot a + \nu \cdot b + \eta \cdot c$, where $a = g_u \circ R_{(u,v)}(s_u(u))$, $b = g_u \circ R_{(u,v)}(s_u(v))$, and $c = g_u \circ R_{(u,v)}(s_u(w))$. In other words, $\triangle = [a, b, c]$ is either the lower or the upper triangle that encloses half of the canonical sector in Figure 4. Next, we map q to Ω_u, Ω_v, and Ω_w using $R^{-1}_{(u,v)} \circ g_u^{-1}$, $R^{-1}_{(v,u)} \circ g_v^{-1}$, and $R^{-1}_{(w,u)} \circ g_w^{-1}$, respectively. By construction, at least one of $R^{-1}_{(u,v)} \circ g_u^{-1}(q)$, $R^{-1}_{(v,u)} \circ g_v^{-1}(q)$, and $R^{-1}_{(w,u)} \circ g_w^{-1}(q)$ is guaranteed to be inside C_u, C_v, and C_w, respectively. Without loss of generality, assume that C_u contains $r = R^{-1}_{(u,v)} \circ g_u^{-1}(q)$. So, we compute the point $s = \theta_u(r) \in S$. This point can be viewed as the counterpart of point $p \in \mathcal{T}$.

The input of our implementation consists of $\mathcal{T}$ and S'. In our experiments, we defined the surface S' either as a PN triangle surface [28] or a Loop subdivision surface [29]. In the latter case, we replaced the function b_σ with the algorithm for exact evaluation of Loop subdivision surfaces at any parameter point of its base mesh, $\mathcal{T}$ (see [30]).

7.1. Examples

We ran the aforementioned implementation of our code on the mesh models in Table 1. For each mesh, we generated two parametric pseudo-surfaces (PPSs), one of which approximates a PN triangle surface defined from the mesh, while the other one approximates a Loop subdivision surface defined on the mesh. Table 2 shows the CPU time for the construction of each PPS, which is highly dominated by the least squares procedure that computes the control points of the shape functions. This procedure is executed n_v times, where n_v is the number of vertices of the input mesh model. Each execution solves a system of about $4 \cdot (m_u + 1)^2$ linear equations using LU decomposition and substitution, where m_u is the valence of the vertex associated with the shape function. Later, we used our method for placing a point on a PPS to sample the PPSs in a triangle midpoint

subdivision manner. We did the same for sampling the corresponding PN triangles and subdivision surfaces.

Model ID	n_v	n_e	n_f	n_h	n_C
1	172	512	344	1	1
2	50	144	96	0	1
3	3,674	11,016	7,344	0	1
4	60,880	183,636	122,424	173	7

Table 1: Mesh model identifier (first column) and the number of vertices (second column), edges (third column), faces (fourth column), holes (fifth column), and connected components (sixth column) of the mesh.

Model ID	Approximated surface	CPU time (ms)
1	PN triangle	3,025
1	Loop	1,640
2	PN triangle	786
2	Loop	446
3	PN triangle	65,800
3	Loop	34,128
4	PN triangle	1,223,128
4	Loop	609,129

Table 2: CPU time in milliseconds for the construction of the PPS surfaces from the models in the first column and the approximated surfaces in the second column. The timing was measured on a single Mac 1.83 Hz Intel Core Duo CPU machine with 1 Gb RAM and running Mac OS X.

Figure 9 shows the mesh models in Table 1. Figures 10-13 show Gaussian curvature plots for the PN triangle, Loop subdivision, and parametric pseudo-surfaces in Table 2. These plots demonstrate two important features of our pseudo-surfaces. First, they show that our PPSs "mimic" closely the shape of the PN triangle or Loop subdivision surface being approximated, which are somewhat different from each other. Secondly, they also show the smoothing effect of the PPSs around the vertices and edges of the PN triangles surfaces and around the extraordinary vertices of the Loop subdivision surfaces. In general, PN triangles surfaces are only C^0-continuous around their vertices and edges. In turn, Loop subdivision surfaces may present curvature continuity problems at extraordinary vertices (the curvature can be zero).

8. Conclusions and Ongoing Work

In this article we have introduced a new manifold-based construction for fitting a smooth surface to a triangle mesh of arbitrary topology. Our construction combines in the same framework most of the best features of previous constructions, and thus it fills the gap left by other methods. More specifically, the manifold structure produced by our construction is more compact and effective than the ones in [15, 16], because it has only one type of p-domains and transition functions, and the transition functions are simpler. Our construction shares several desirable properties with the one in [17], including the ability for producing C^∞-continuous surfaces and the flexibility in ways of defining their geometry. However, differently from the construction in [17], ours generates surfaces from triangle meshes, rather than quadrilateral meshes, and the surfaces are contained in the convex hull of all control points used to define their geometry. Unlike the surfaces produced by the construction in [18], the ones produced by our construction are not given by purely (rational) polynomial functions. However, our surfaces are C^∞-continuous everywhere, while the ones generated in [18] may present singularities.

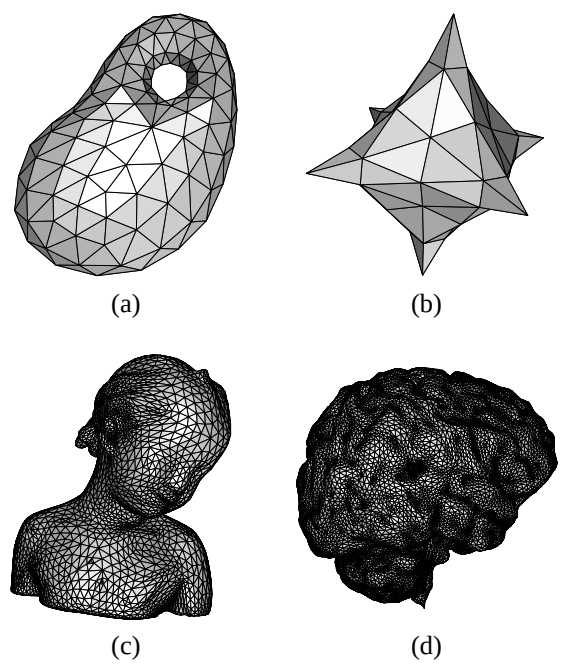

Figure 9: Mesh models (a) 1, (b) 2, (c) 3, and (d) 4 from Table 1.

Finally, our construction is based on a solid theoretical framework, which ensures its correctness, and we provided experimental examples of the surfaces generated by our construction. In particular, the results in Section 7 show that our construction can be combined with parametric and subdivision schemes to offer the user a "black-box" procedure to generate a C^∞ surface from a small or large triangle mesh. We believe that

our construction can be very useful for applications in need of a "black-box" procedure to fit a higher-order continuous surface, *given by an analytic expression*, to a triangle mesh.

We are currently working on the problem of adaptively fitting C^∞ surfaces to dense triangle meshes. To this end, we are developing a new solution to the fitting problem that closely approximates meshes with a very large number of vertices by a smooth pseudo-parametric manifold containing a small number of charts. We also plan to extend this adaptive fitting algorithm to generate a hierarchical manifold structure that can represent surfaces in multiresolution. In addition, we intend to further investigate the existence of (rational) polynomial transition functions that can replace the ones currently used by our construction.

Acknowledgments

We would like to thank Jos Stam for making available to us his own implementation of the algorithm in [30]. All mesh models used in Section 7.1 are provided courtesy of INRIA and MPII by the AIM@SHAPE repository, except for Model 1.

References

[1] G. Farin, Curves ans Surfaces for CAGD: A Practical Guide, 5th Edition, Morgan-Kaufmann, 2002.

[2] G. Greiner, H.-P. Seidel, Modeling with Triangular B-Splines, IEEE Computer Graphics and Applications 14 (2) (1994) 56–60.

[3] H. Prautzsch, G. Umlauf, Parameterization of triangular g^k spline surfaces of low degree, ACM Transaction on Graphics 25 (4) (2006) 1281–1293.

[4] E. Catmull, J. Clark, Recursively Generated B-Spline Surfaces on Arbitrary Topological Surfa ces, Computer-Aided Design 10 (6) (1978) 350–355.

[5] D. Doo, M. Sabin, Behaviour of Recursive Division Surfaces Near Extraordinary Points, Computer-Aided Design 10 (6) (1978) 356–360.

[6] C. T. Loop, Smooth Subdivision Surfaces Based on Triangles, Master's thesis, Department of Mathematics, University of Utah, Salt Lake City, Utah, USA (1987).

[7] N. Dyn, D. Levine, J. A. Gregory, A Butterfly Subdivision Scheme for Surface Interpolation with Tension Control, ACM Transactions on Graphics 9 (2) (1990) 160–169.

[8] J. Peters, U. Reif, The Simplest Subdivision Scheme for Smoothing Polyhedra, ACM Transactions on Graphics 16 (4) (1997) 420–431.

[9] L. Kobbelt, $\sqrt{3}$ Subdivision, in: Proceedings of the 27th annual conference on Computer graphics and interactive techniques (SIGGRAPH '00), New Orleans, Louisiana, USA, 2000, pp. 103–112.

[10] L. Velho, D. Zorin, 4-8 Subdivision, Computer Aided Geometric Design 18 (5) (2001) 397–427.

[11] J. Peters, U. Reif, Shape Characterization of Subdivision Surfaces – Basic Principles, Computer Aided Geometric Design 21 (6) (2004) 585–599.

[12] K. Karciauskas, J. Peters, U. Reif, Shape Characterization of Subdivision Surfaces – Case Studies, Computer Aided Geometric Design 21 (6) (2004) 601–614.

[13] H. Prautzsch, U. Reif, Degree Estimates for C^k Piecewise Polynomial Subdivision Surfaces, Advances in Computational Mathematics 10 (2) (2004) 209–217.

[14] U. Reif, A Degree Estimate for Subdivision Surfaces of Higher Regularity, Proceedings of the American Mathematical Society 124 (7) (2006) 2167–2174.

[15] C. M. Grimm, J. F. Hughes, Modeling Surfaces of Arbitrary Topology Using Manifolds, in: Proceedings of the 22nd ACM Annual Conference on Computer Graphics and Interactive Techniques (SIGGRAPH 95), ACM, 1995, pp. 359–368.

[16] J. C. Navau, N. Pla-Garcia, Modeling Surfaces from Meshes of Arbitrary Topology, Computer Aided Geometric Design 7 (1) (2000) 643–671.

[17] L. Ying, D. Zorin, A Simple Manifold-Based Construction of Surfaces of Arbitrary Smoothne ss, ACM Transactions on Graphics 23 (3) (2004) 271–275.

[18] X. Gu, Y. He, H. Qin, Manifold Splines, Graphical Models 68 (3) (2006) 237–254.

[19] C. M. Grimm, D. Zorin, Surface Modeling and Parameterization With Manifolds, in: ACM SIGGRAPH 2006 Courses (SIGGRAPH '06), ACM Press, New York, NY, USA, 2006, pp. 1–81.

[20] C. M. Grimm, J. J. Crisco, D. H. Laidlaw, Fitting Manifold Surfaces to Three-Dimensional Point Clouds, Journal of Biomechanical Engineering 124 (1) (2002) 136–140.

[21] J. C. Navau, N. Pla-Garcia, M. Vigo-Anglada, A Generic Approach to Free Form Surface Generation, in: Proceedings of the 2002 ACM Symposium on Solid Modeling (SM'02), 2002, pp. 35–44.

[22] J. Milnor, J. D. Stasheff, Characteristic Classes, Vol. 76 of Annals of Mathematics Studies, Princeton University Press, 1974.

[23] X. Gu, Y. He, M. Jin, F. Luo, H. Qin, S. ng Tung Yau, Manifold Splines with Single Extraordinary Point, Computer-Aided Design 40 (6) (2008) 676–690.

[24] M. Botsch, M. Pauly, C. Rössl, S. Bischoff, L. Kobbelt, Geometric Modeling Based on Triangle Meshes, in: SIGGRAPH Course Notes, ACM, 2006.

[25] M. Berger, B. Gostiaux, Differential Geometry, Manifolds, Curves, and Surfaces, Vol. 115 of GTM, Springer-Verlag, 2006.

[26] M. Siqueira, D. Xu, J. Gallier, Construction of c^∞ surfaces from triangular meshes using parametric pseudo-manifolds, Tech. rep., University of Pennsylvania, `http://repository.upenn.edu/cis_reports/877` (2008).

[27] M. de Berg, M. van Kreveld, M. Overmars, O. Schwarzkopf, Computational Geometry: Algorithms and Applications, 2nd Edition, Springer-Verlag, 2000.

[28] A. Vlachos, J. Peters, C. Boyd, J. L. Mitchell, Curved PN triangles, in: Proceedings of the ACM Symposium on Interactive 3D Graphics, Research Triangle Park, NC, USA, 2001, pp. 159–166.

[29] C. T. Loop, A G^1 Triangular Spline Surface of Arbitrary Topological Type, Computer Aided Geometric Design 11 (3) (1994) 303–330.

[30] J. Stam, Evaluation of Loop Subdivision Surfaces, in: ACM SIGGRAPH 1999 Courses (SIGGRAPH '99), ACM Press, New York, NY, USA, 1999, pp. 1–15.

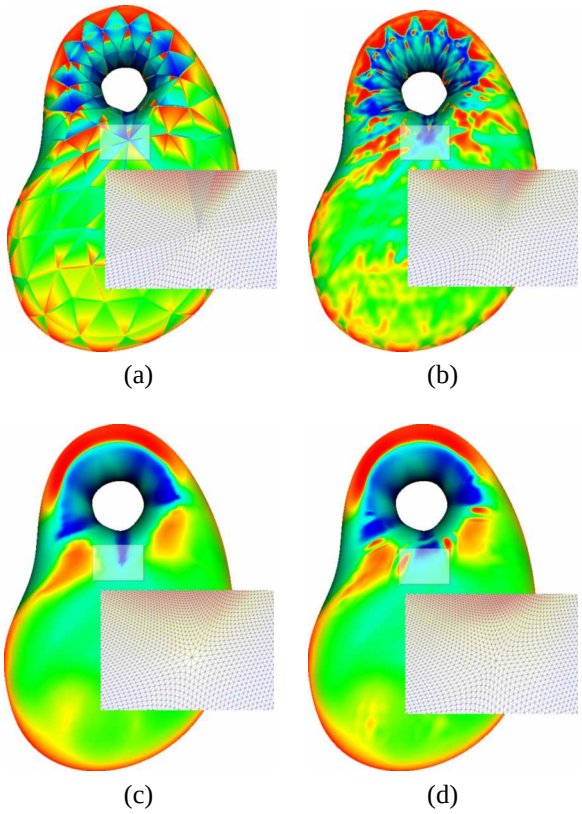

Figure 10: Curvature plots for the surfaces generated from mesh model 1: (a) PN triangle, (b) PPS from the surface in (a), (c) Loop, and (d) PPS from the surface in (c).

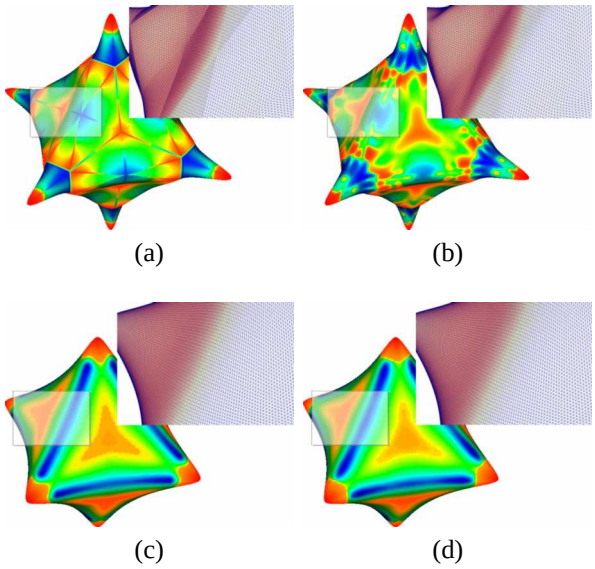

Figure 11: Curvature plots for the surfaces generated from mesh model 2: (a) PN triangle, (b) PPS from the surface in (a), (c) Loop, and (d) PPS from the surface in (c).

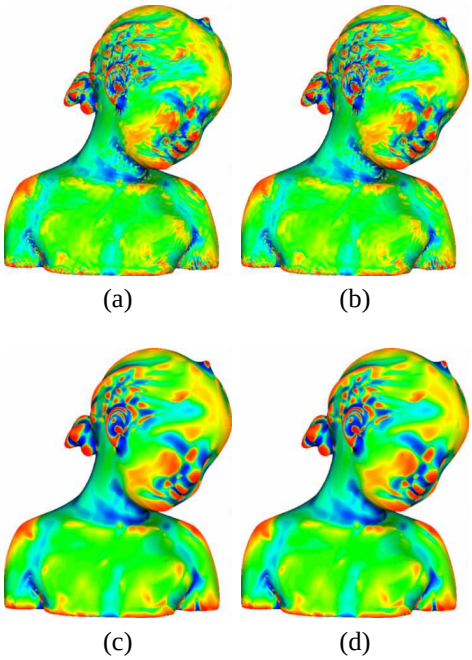

Figure 12: Curvature plots for the surfaces generated from mesh model 3: (a) PN triangle, (b) PPS from the surface in (a), (c) Loop, and (d) PPS from the surface in (c).

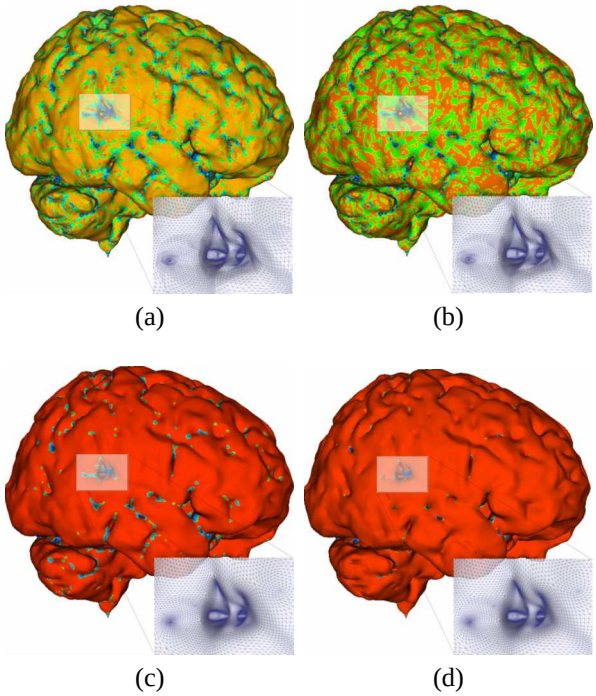

Figure 13: Curvature plots for the surfaces generated from mesh model 4: (a) PN triangle, (b) PPS from the surface in (a), (c) Loop, and (d) PPS from the surface in (c).